The final publication is available at Elsevier via https://dx.doi.org/10.1016/j.electacta.2018.02.098 © 2018. This manuscript version is made available under the CC-BY-NC-ND 4.0 license https://creativecommons.org/licenses/by-nc-nd/4.0/

# Accepted Manuscript


Acrylonitrile copolymer/graphene skinned cathode for long cycle life rechargeable hybrid aqueous batteries at high-temperature

Jian Zhi, Koen Bertens, Alireza Zehtab Yazdi, P. Chen

PII: S0013-4686(18)30393-1

DOI: 10.1016/j.electacta.2018.02.098

Reference: EA 31293

To appear in: *Electrochimica Acta*

Received Date: 8 November 2017

Revised Date: 17 February 2018

Accepted Date: 19 February 2018

Please cite this article as: J. Zhi, K. Bertens, A.Z. Yazdi, P. Chen, Acrylonitrile copolymer/graphene skinned cathode for long cycle life rechargeable hybrid aqueous batteries at high-temperature, *Electrochimica Acta* (2018), doi: 10.1016/j.electacta.2018.02.098.

This is a PDF file of an unedited manuscript that has been accepted for publication. As a service to our customers we are providing this early version of the manuscript. The manuscript will undergo copyediting, typesetting, and review of the resulting proof before it is published in its final form. Please note that during the production process errors may be discovered which could affect the content, and all legal disclaimers that apply to the journal pertain.

ACCEPTED MANUSCRIPT

# Acrylonitrile Copolymer/Graphene Skinned Cathode for Long Cycle Life Rechargeable Hybrid Aqueous Batteries at High-Temperature

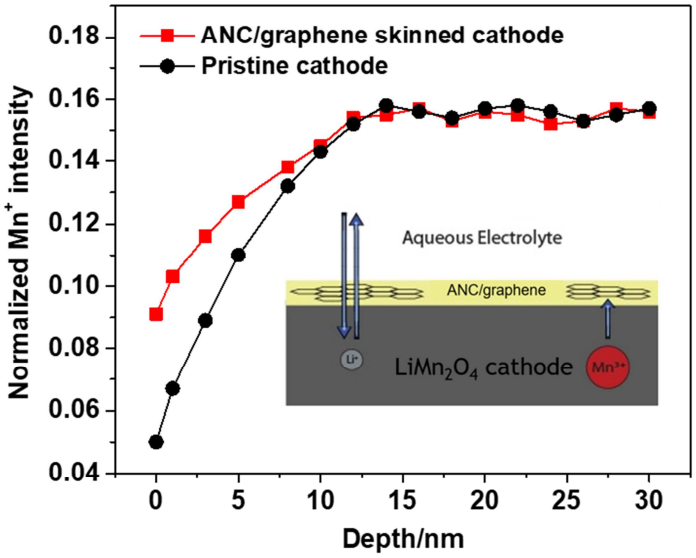


ACCEPTED MANUSCRIPT

ACCEPTED MANUSCRIPT

# Acrylonitrile Copolymer/Graphene Skinned Cathode for Long Cycle Life Rechargeable Hybrid Aqueous Batteries at High-Temperature

*Jian Zhi,† Koen Bertens,† Alireza Zehtab Yazdi, P. Chen**

*Department of Chemical Engineering and Waterloo Institute for Nanotechnology, University of Waterloo, 200 University Avenue West, Waterloo, Ontario N2L3G1, Canada*
*†These authors contributed equally to this work.*
**Email: p4chen@uwaterloo.ca*

**Abstract**

For aqueous rechargeable lithium battery (ARLB), excellent cycling stability at elevated temperature is highly desirable in its application of electric vehicles (EVs). However, most state-of-art ARLBs show poor durability under high-temperature operation. Herein, we demonstrate a facile coating approach that can construct a thin acrylonitrile copolymer (ANC)/graphene skin on the top-surface of the $LiMn_2O_4$ (LMO) cathode in a rechargeable hybrid aqueous lithium battery (ReHAB). Featuring the continuous coverage and the facile electron transport, the ANC/graphene skinned cathode shows a capacity retention of 61% after 300 cycles at 60 °C, two times larger than the battery without the skin. In the cathode, ANC helps to suppress unwanted interfacial side reactions, and graphene renders a robust ion diffusion framework. Quantitative analysis of Mn suggests that the ANC/graphene skin can greatly suppress dissolution of Mn from the LMO into the aqueous electrolyte, while maintaining the charge transfer kinetics. The polymer-based nanocomposite skin on small (1.15 mAh cell) and large (7 mAh cell) cathodes show similar electrochemical improvement, indicting good scale-up potentials.

## 1. Introduction

Compared with other commonly used batteries, lithium-ion batteries (LiBs) are featured by high energy and power density, and thus have been successfully applied in electronic vehicles (EVs).[1, 2] However, the relatively high operating temperature (up to 60°C) of cells in EVs will lead to the decomposition of organic electrolyte, produce combustible gas and therefore pose potential security risks.[1] To tackle this problem at their root, the aqueous rechargeable lithium battery (ARLB) was first proposed in 1994,[3] and has drawn significant attentions.[4-7] Recently, spinel $LiMn_2O_4$ (LMO) has demonstrated promising potentials as a cathode material for ARLBs. Stems from its three-dimensional $Li^+$ diffusion channels, LMO based ARLB can deliver more power in comparison with $LiFePO_4$, $LiCoO_2$ and $LiNi_{1/3}Co_{1/3}Mn_{1/3}O_2$.[8-10] The serious capacity fading of the LMO-based ARLBs at high temperatures (50-60°C), however, still significantly limits their practical applications in EVs. Such capacity fading is mainly owing to the accelerated manganese dissolution from cathode into the aqueous electrolyte.

Extensive studies have been conducted to suppress Mn dissolution to improve long-term stability of the LMO-based ARLB systems. One method to overcome this issue is surface modification using inorganic metal oxides, such as $SiO_2$,[11] MgO,[12] ZnO,[13, 14] $ZrO_2$,[15] and Co-Al mixed metal oxide,[16] most of which focus on restriction of the side reactions between the LMO and the aqueous electrolyte. Since there is insufficient contact between the adjacent LMO particles, the inorganic compounds cannot cover the entire electrode surface.[17] Moreover, they are often electrochemically inert, and their negligible capacities deteriorate the overall gravimetric capacity of the batteries, leading to the significantly reduced energy density.

$Li^+$ penetrable acrylonitrile copolymer (ANC) coating in the Li-S batteries has been recently shown as a promising method of suppression of the interfacial side reactions of the LMO particles that can enhance the cycle life.[18] Inspired by the successful application of ANC in the

Li-S systems, here we report a facile and fully scalable method to coat the surface of the LMO particles with ANC. A sub-micron ANC/graphene skin layer is coated on the top-surface of the LMO cathode, and is tested in a rechargeable hybrid aqueous lithium battery (ReHAB).[19-21] The coating method is based on an air-spraying system that can control the thickness (200 nm to 1μm) of the skin layer on a given surface area (1 $cm^2$ to 1 $m^2$). Battery testing under 60 °C shows that the ANC/graphene skinned cathode (300 nm in thickness) shows a capacity of 61% after 300 cycles, which is superior than the most reported values in the literature for the LMO-based cathode at elevated temperature. More notably, such hybrid skin on a large (~ 9 $cm^2$ in 7 mAh cell) cathode also showed high capacity retention (51.3% compared to initial capacity) after 500 cycles under 60°C, 120% higher compared to the pristine cathode (23.4% of the initial capacity). We hypothesize that in such hybrid skin, ANC suppresses the unwanted interfacial side reactions while graphene renders a robust ion diffusion framework. Extensive impedance analysis and quantitatively evaluation of Mn content on the LMO surface are employed to study the key roles of the ANC/graphene skin.

## 2. Experimental

X-ray diffraction (XRD) was conducted using a Bruker D8-Disc x-ray diffractometer with a wavelength of 1.54 Å and Cu X-ray Tube. SEM was conducted in a Philips XL30 ESEM. The dissolved Mn in the liquid electrolyte was quantitatively monitored along with cycle number and storage time using inductively coupled plasma optical emission spectroscopy (ICP-OES, OPTIMA 7300 DV, PerkinElmer). Depth profiles were obtained employing a TOF-SIMS 5 spectrometer (IonTof), which was conducted at a pressure of $\sim 1 \times 10^{-9}$ mbar. A pulsed 25 keV $Bi^+$ primary ion source was used for analysis, delivering 1.8 pA of current over a 100 μm × 100

μm area. Sputtering was done using a 2 keV $Cs^+$ beam giving a 100 nA target current over a 250 μm × 250 μm area.

Cathodes were created by casting a slurry of $LiMn_2O_4$ powder, KS6 graphite powder, and polyvinylidene fluoride in n-methyl-2-pyrrolidinone onto polyethylene film and air drying at reduced pressure at 60 degrees Celsius for 24 hours. These cathodes were spray coated using the Wagner FLEXiO 590 Sprayer. A solution of 1 mg/mL graphene flakes, suspended in 11.7 % w/w solution of ANC aqueous binder, was spray coated directly onto the cathode. Spray times of 2 seconds, 5 seconds, and 10 seconds were used, and distance from nozzle to cathode was varied between approximately 15 cm, 30 cm, and 60 cm. The result was nine different samples, as well as a blank sample, to evaluate under float charge testing.

ReHABs (coin cell) were assembled to test battery performance. Disks were cut from the cathode with a diameter of 12 mm. Metallic zinc plates of the same diameter were used as the anode, and AGM (Absorbed Glass Mat) was used as a separator. The electrolyte used was a solution of 2M $ZnSO_4$, 1M $Li_2SO_4$, dissolved in DI water and titrated to pH 4 using 0.1M LiOH. Similarly, 7 mAh big cells were assembled employing 5 cm × 5 cm stainless-steel sheet as external shells and thermal conductive rubber as spacer. The area of cathode and anode is 2 cm × 2 cm and 4 cm × 4 cm, respectively. Cyclic voltammetry (CV) was performed on a Biologic-VMP3 electrochemical workstation. Electrochemical impedance spectroscopy (EIS) was conducted on CHI 660D electrochemical workstation, using Pt, Ag/AgCl and 1M $Li_2SO_4$/2M $ZnSO_4$ as counter electrode, reference electrolyte and electrolyte, respectively. Charge-discharge cycling test was performed at room temperature and 60°C, using a Neware battery tester at 4C (1 C=120 mA $g^{-1}$) between 1.4 and 2.1 V. Rate capability test was performed under 1C to 10C. Float charge tests were conducted by charging the cell to 2.1 V and holding it for 24 hours. To

measure the ionic conductivity, the skin (4 $cm^2$) was sandwiched between two stainless-steel electrodes and soaked in aqueous electrolyte (2M $ZnSO_4$ and 1M $Li_2SO_4$) in 2032 coin type cell. The impedance measurement was performed using a Biologic-VMP3 electrochemical workstation over a frequency range of 0.1 Hz–1 MHz with an amplitude of 10 mV. Each sample was equilibrated for 1 h before measurement. The conductivity was calculated by the relation $\sigma = d/SR$, where 1/R is the conductance to be determined from the admittance plots, d is the thickness of the sample and S is the cross-sectional area of each electrode.

Float charge test results showed the lowest capacity loss came from spraying the cathode for 2 seconds at 15 cm distance and 10 seconds at 30 cm distance (Figure S1). These methods would allow for a moderate amount of coating deposited on the cathode compared to other methods. To reduce resource consumption, further tests were run using a spray time of 2 seconds and a distance of 15 cm. Further tests were done by coating the cathode with solutions of graphene flakes suspended in DI water and ANC solution at 1 mg/mL. A blank cathode and a cathode coated with ANC solution were also prepared. The cathode performance was tested using float charge testing, cyclability testing, and C-rate testing.

## 3. Results and Discussion

**Figure 1**. (a-c) SEM images of pristine, ANC skinned and ANC/graphene skinned cathodes, respectively. (d) TEM image of ANC/graphene skin.

Before evaluating electrochemical performance of LMO based ReHABs, the surface structure of ANC/graphene skinned LMO cathode was comprehensively characterized. The SEM images show that compared with the pristine LMO cathode having obvious edges (Figure 1a), the

successfully wrapping of ANC skin features a highly continuous morphology (Figure 1b). The acrylonitrile groups in ANC have high polarity, which ensures the firm affinity for LMO.[22] The SEM image of the ANC/graphene (with a mass ratio of 1:2) skinned LMO cathode is shown in Figure 1c, wherein some areas the composite skin shows mainly an irregular morphology with multiple shapes including both layer and gum-like structures. Graphene is interconnected with the polymer network. As indicated in Figure 1c, graphene flakes can be seen embedded in the ANC. The unusual hybrid wrapping layer was further characterized by TEM. Amorphous ANC fine particles are attached firmly onto the graphene sheets, which shows a transparent silk-like structure (Figure 1d). To investigate the thickness of such hybrid skin on the cathode, we coated ANC/graphene on a flat silica substrate, employing the same spraying method. From the cross-sectional SEM image of ANC/graphene coated silica (Figure S2), we determine that the thickness of ANC/graphene skin is only 300 nm. Through changing the spraying time, the thickness of ANC/graphene skin can be easily changed, ranging from 200 nm to around 1 μm (Figure S3). As ANC shows similar binding affinity on silica and LMO surfaces,[23, 24] we can estimate the thickness of ANC/graphene skin on our ReHAB cathode. Schematic illustrations of this ANC/graphene skin formed on LMO cathode and its role as a protective layer to suppress the side reactions are exhibited in Scheme 1.

**Scheme 1**. Schematic illustration of ANC/graphene skin on the surface of LMO cathode and its role in suppressing the undesired interfacial reactions.

Figure 2a shows the X-ray diffraction (XRD) patterns of pure ANC and ANC/graphene skins, as well as graphene. The XRD spectrum of ANC skin shows a sharp peak and a weak diffraction peaks at 16.5° and 28.5°, respectively. The first peak is indexed to (100) diffraction of hexagonal lattice of ANC, while the second peak belonged to the second-order diffraction of the first peak.[25] After the introduction of graphene, the XRD pattern of ANC/graphene skin presents an extra peak (26.4°), belonging to the (002) reflection of graphene,[26] while still preserving the ANC peaks. According to the XRD results, it is clear that our spray-coating method did not change the structure of graphene and ANC chains. The XRD patterns of the ANC/graphene skinned LMO cathode were compared with those of ANC skinned and the pristine LMO cathodes (Figure 2b). The Fd3m space group, where lithium ions occupy the tetrahedral sites and Mn resides at the octahedral site, can be seen in all the three samples. Both pristine and skinned LMO show very close lattice parameters (i.e., a= 8.1672 Å for pristine LMO cathode and a=8.1663 Å for ANC/graphene skinned LMO cathode), which are consistent in previous studies.[27] Such quantitative characterization of XRD patterns indicates that the introduction of ANC/graphene skin does not impact the spinel crystalline structure of LMO. It is noteworthy that owing to the high intensity from LMO and graphite substrate in the cathode, the peaks belonging to ANC and graphene are completely overlapped, which makes it difficult to characterize ANC/ANC skin in such cathode-based spectrum.

**Figure 2**. (a) XRD patterns of ANC, ANC/graphene skin and graphene. (b) XRD patterns of pristine LMO cathode, as well as ANC and ANC/graphene skinned LMO cathodes.

The effects of ANC/graphene skin on the electrochemical performance of the cathode in ReHAB are evaluated in detail. The cyclic voltammetry (CV) results of ANC and ANC/graphene

skinned cathodes are presented on Figure 3a. All currents are normalized to the electrode loadings. In the CV results, there are two distinctive pairs of reduction/oxidation peaks, which correspond to the two steps of intercalation/deintercalation of $Li^+$ into/out of LMO lattice. It is observed that there is only a slight increase in polarization in skinned cathodes compared to that of the pristine sample, suggesting that the kinetics of electrochemical reactions in these cathodes are not significantly altered. Figure 3b-c depicts the effect of ANC and ANC/graphene skin on the discharge profiles of ReHAB under different discharge rate (1 C to 10 C). No abnormal discharge curves can be seen in either the ANC, or the ANC/graphene skinned LMO cathode. The discharge curves present two distinguished plateaus, which reflect two-stage Li ion insertion behavior and are consistent with the obtained CV data. The ANC and ANC/skinned cathodes show a similar discharge capacity of 110 mA h $g^{-1}$ at a current density of 0.5 C. The gradually decreasing of discharge capacity with an increase of current density clearly addresses the influence of ohmic polarization on battery performance.

During the discharge, $Li^+$ needs to migrate from the solvent to the cathode.[28] Consequently, a fast ion transfer in electrolyte/electrode interface is highly required. As the introduction of an extra layer on electrode surface inevitably adds some barriers for ion transfer, high ionic conductivity of the coating is crucial to ensure the efficient $Li^+$ migration.[29, 30] In this study, ANC skin exhibits an ionic conductivity of 0.56 mS $cm^{-1}$, which is highly comparable with the value of the polymer electrolyte.[31-33] Therefore, $Li^+$ transport after the skinning is not likely to be hampered, and ANC skinned cathode shows comparable discharge capacities and C-rate capability as pristine cathode (Figure 3d). To investigate the swelling behavior of ANC/graphene skin by electrolyte solution, we spray coated ANC/graphene on a flat silica substrate and immerse the sample into aqueous electrolyte (2M $ZnSO_4$ and 1M $Li_2SO_4$) for 24 hours at 20°C.

Evidenced by the cross-sectional SEM image shown in Figure S4, the average thickness of ANC/graphene skin increased from 300 nm to 420 nm after 24 hours aging in aqueous electrolyte, indicating a 40% volume swelling. The abundant hydrophilic acylamino/cyano groups from ANC can absorb large amount of aqueous electrolyte, which is the main reason for such swelling behavior. Owing to its high liquid electrolyte uptake capability, the Li ion transfer inside the coating layer is supported by aqueous electrolyte, and thus ensure a fast Li ionic flux compatible in bulk solution. Moreover, the hydrophilic functional groups (OH, COOH, and C-O-C) in graphene can adsorb water molecules and support both the upstream and downstream fluxes of $Li^+$,[34] which further facilitate ion diffusion and accelerate the electrochemical kinetics in the interface between electrolyte and cathode. Figure S5 shows the 10C discharge capacity of ANC/graphene skinned cathodes under different ANC/graphene ratio. It is clear that the cathode skinned with 1:2 ANC/graphene mass ratio exhibits the highest capacity. After further increasing the amount of graphene, the capacity of skinned cathodes decreased to some extent. The agglomeration of graphene leads to the formation of a discontinuous layer, which may block $Li^+$ transportation and penetration into LMO, and the ideal features of the skin would not be obtained.

**Figure 3**. (a) Cyclic voltammetry (CV) results of ANC and ANC/graphene skinned cathodes, in comparison with pristine cathode. (b,c) Discharge profiles of ANC and ANC/graphene skinned cathodes. (d) Comparison of discharge C-rate capabilities of ANC and ANC/graphene skinned cathodes with pristine one.

The effect of ANC/graphene skin on the cycle performance of ReHAB cathode at 4C under a potential range from 1.4 to 2.1V was investigated, wherein both cells exhibit similar capacity

under this C-rate (Figure 3d). ANC/graphene skinned cathode exhibits similar discharge capacities with pristine cathode after 300$^{th}$ cycles in room temperature, and the coresponding capacity retentions of the pristine and ANC/graphene skinned cathodes are 76.4% and 73.8%, respectively (Figure 4a). However, enormous different cycle behavior can be seen under 60 °C. As shown in Figure 4b, ANC/graphene skinned cathode presents the significantly improved cycle life in comparison to pristine cathode. In the initial few cycles, there is slight difference in the retentions between the two cathodes. As the cycle number increases, pristine cathode shows a low capacity retention of around 20% after 300 cycles. In contrast, the capacity retention of the ANC/graphene skinned cathode after 300 cycles is observed to be 61%, which is 200% larger than the value in pristine cathode. Figure S6 shows the XRD patterns of powders scraped from ANC/graphene skinned cathode after 300 cycles at 60°C. Compared with the XRD patterns of the LMO powders without cycling, it can be concluded that the LMO active material from the cycled batteries retains its structural characteristics. All the peaks are well indexed with spinel $LiMn_2O_4$. However, minor changes in relative peak intensities and peaks broadening are observed, indicating the inevitable deterioration of active mass in cathode during high-temperature cycling.[35]Such significantly improved cycle life indicates that, owing to the efficient protection of ANC/graphene skin to LMO cathode, the undesired side reaction between LMO cathode and aqueous electrolyte is greatly suppressed. Table 1 summarizes a comparison of cycle life performance of ANC/graphene skinned LMO cathode with the previous literature data for various kinds of lithium batteries. [19, 36-43]

**Table 1**. A comparison of the cycling stability of various rechargeable lithium battery systems under elevated temperature

**Figure 4**. (a,b) Discharge capacities along with cycle number for ReHABs with pristine or ANC/graphene skinned cathodes: (a) at room temperature; (b) at 60°C. (c) Cyclability of 7 mAh ReHAB assembled with pristine or ANC/graphene skinned cathodes at 60°C.

The spray-coating method was also employed to fabricate the ANC/graphene skin on the large area (7 mAh cell, 9 $cm^2$ ) cathodes, as shown in Figure S7. ANC/graphene skinned large area-cathode also showed high capacity retention (51.3% compared to initial capacity, Figure 4c) after 500 cycles under 60°C, 32% improvement compared to the pristine cathode (23.4% of the initial capacity). Compared with coin cell, it is obvious that 7 mAh battery shows much better cycling stability in both skinned and pristine samples under elevated temperature. Such difference in battery performance is mainly derived from their different internal structures. In coin cell, stainless-steel spring was used to ensure the close electrical contact of electrodes, separator and external shells. As only limited area of spring is in contact with separator-electrode stack, the heat removal from the electrode to the exterior shell is inadequate. When the cells are cycled under elevated temperature, the extra heat generated from the side reactions accumulates in the electrode and results in large temperature rise within the cell.[44] The additional overheating of the cell accelerates Mn dissolution from the cathode to electrolyte, which further deteriorate the cycling performance. After skinning with ANC/graphene, the restriction of the side reactions between the LMO and the aqueous electrolyte significantly suppresses the heat generation in the electrode, and the cells shows lower internal temperature than pristine cell. Considering largely decreased Mn dissolution as discussed in the manuscript, there is no doubt that ANC/graphene skinned cathode exhibits much higher capacity retention compared with pristine cathode. In 7

mAh large cells, the electrodes and separator are packed with 5 cm × 5 cm stainless-steel sheet and thermal conductive rubber. The large thermal contact area ensures adequate heat transfer, resulting in much larger thermal conductance than in coin cell.[45] The internal heat generated from side reactions can be immediately transferred to the external shell, significantly reducing the overheating problem. Consequently, the cathodes in 7 mAh cell shows much better cycling performance than that in the coin cell. As shown in Figure S8, ANC/graphene skinned cathode shows similar cycle life as pristine cathode, which is in consistent with coin cell results under room temperature (25 °C , Figure 4a). Moreover, there is no significant difference in cycling performance between coin cells (Figure 4a) and 7 mAh cells (Figure S8). All these results clearly indicate that such overheating phenomenon in coin cells only occurs under elevated temperature. In room temperature, the kinetics of electrochemical processes are relatively slow.[46] The generated heat is negligible and cannot affect the performance of aqueous batteries.

Figure S9 shows the coulombic efficiencies of ANC/graphene skinned and pristine cathodes in 7 mAh cell. under 60°C, it is well known that the dendrite formation in the anode can be greatly accelerated, leading to the drastic deterioration of coulombic efficiency. However, ANC/graphene skinned large area-cathode still maintained 87% coulombic efficiency after 200 cycles, while the value in pristine cathode decreased to 56%. SEM images of Zn anodes from 7 mAh cells after 300 cycles under 60°C are shown in Figure S10. The Zn electrode cycled with pristine cathode showed extensive mossy-like dendrite formation (Figure S10a). The surface of anode is rough, and many large holes can be observed. It has previously been shown that the mossy-like metal dendrite will produce a dead metal layer and become electrically isolated during cycling and results in low columbic efficiency as well as increased polarization.[47] In contrast, the Zn anode with ANC/graphene cathode exhibited rather smooth morphologies

without any visible dendrite growth, as shown in Figure S10b. At present the impact of cathode coating on the dendrite formation in anode is not clear, and related mechanisms are under studied in our group. ANC is the key contribution to protect cathode from undesired side reactions. Figure S11 shows the cycling performance of 7 mAh cell with graphene coated cathode under 60°C. After 300 cycles, capacity retention of the cell is only 27%, which is similar as pristine sample. Without ANC, graphene itself cannot form homogeneous skin on cathode surface. The aggregation of graphene particles makes such coating impossible to protect the electrode well.

This superior high-temperature cycle life of ANC/graphene skinned cathode was further evaluated by testing the Mn dissolution amount (via ICP-AES) at 60°C as a function of cycle numbers (300 cycles). According to Hunter's reaction, LMO is not stable in an acidic medium undergoing the following decomposition:

$$2LiMn_2O_4 + 4H^+ \rightarrow 3\lambda\text{-}MnO_2 + Mn^{2+} + 2Li^+ + 2H_2O$$

Such dissolution process may continue because $Li^+$ and $Mn^{2.5+}$ in the bulk can diffuse to the surface, and become more pronounced at elevated temperatures. Such Mn dissolution from LMO not only results in the loss of active materials (LMO), but also results in the structural deformation from spinel to a mixed phase with $\lambda$-$MnO_2$, which both greatly impact the cycle life of the cathode. Figure 5a shows that, at both the pristine and the skinned cathodes (assembled in ReHABs with coin cell), the dissolved amounts of Mn into electrolyte determined by ICP-AES is increased. Whereas pristine cathode exhibits higher Mn dissolution (278 ppm) after 300 cycles, a much smaller amount of Mn (128 ppm) was observed in the ANC/graphene skinned cathode, showing a 53% decrease. The amount of Mn dissolution to the electrolyte with storage time was also obtained for delithiated LMO cathodes at 60 °C. In Figure S12, the amount of Mn dissolution increased drastically in the initial 10 days, and finally became steady after 14 days. In

consistent to the dissolution analysis during cycling test, ANC/graphene skinned cathode showed much lower amount of Mn dissolution (198 ppm) than pristine cathode (472 ppm) after 14 days. As a result, it is clear that the ANC/graphene skin is efficient to protect the LMO surface, leading to the retardation of Mn dissolution (scheme 1). Figure S13 shows the Mn dissolution amount at room temperature along with different cycles. Owing to significantly decelerated kinetics in electrochemical reactions, the amount of Mn dissolution during cycling is not as high as that under high-temperature. However, ANC/graphene skinned cathode still shows a smaller amount of Mn dissolution compared with pristine cathode, indicating an efficient protection.

**Figure 5.** (a) Mn dissolution into aqueous electrolyte along with cycle numbers at 60 °C in ReHABs assembled with pristine and ANC/graphene skinned cathodes. (b,c) Changes in AC impedance spectra ($1^{st}$ and $300^{th}$ cycle) of ReHABs fabricated with: (b) pristine and (c) ANC/graphene skinned LMO cathodes. (d) Depth profiles of $Mn^{+}$ content obtained by TOF-SIMS (normalized by that of $Li^{+}$ in pristine and ANC/graphene skinned cathodes.

To further study the advantageous impact of the ANC/graphene skin on high-temperature cycling, the impedance spectra of ReHABs (in coin cell) after the $1^{st}$ and $300^{th}$ charge/discharge cycle were measured (Figure 5b and c). The corresponding equivalent circuit of batteries assembled with LMO cathode is shown in Figure S14. At the low frequency region, the diameter of semicircle represents the charge transfer resistance ($R_{ct}$).[48, 49] Since there is no solid-electrolyte interphase (SEI) layer formed in aqueous lithium batteries,[50, 51] a semicircle at the high frequency region cannot be observed. As shown in Figure 5b, $R_{ct}$ considerably increases by 46 Ohm after the $300^{th}$ cycle in the pristine cathode. The significant increase in impedance may

be caused by the formation of λ-$MnO_2$ derived from the side reaction between the LMO and water in repeated charge/discharge.[13] Compared to LMO, λ-$MnO_2$ shows much inert electrochemical activity and can greatly impair the charge transfer kinetics of $Li^+$.[52, 53] In comparison, for the ANC/graphene skinned cathode, the increase of battery impedance is largely suppressed ($R_{ct}$ increase only by 12 Ohm $cm^2$). The EIS characterizations of the ANC/graphene skinned and pristine cathodes were also conducted over time. The evolution trends of $R_{ct}$ were obtained (Figure S15). In the case of pristine cathode, the $R_{ct}$ value increased over storage time. As the electrolyte properties remained the same over time, the increase in $R_{ct}$ may be attributing to the dissolution of Mn from LMO, and the formation of a $MnO_2$ layer. In contrast, the $R_{ct}$ value of ANC/pristine cathode is relatively stable along with storage time. The EIS results from cycling and aging conditions clearly show that ANC/graphene skinning can effectively protect cathode from direct exposure to aqueous electrolyte. Consequently, λ-MnO2 may be poorly produced in ANC/graphene skinned cathode and the lithium transfer kinetics are not significantly deteriorated. The rate capabilities of cells assembled with ANC/graphene skinned and pristine cathodes under 60 °C is shown in Figure S16. Even at a high rate of 10 C, the cell with ANC/graphene skinned cathode maintained a tenacious capacity of 48 mAh $g^{-1}$. In contrast, the discharge capacity in pristine cell dropped sharply to 31 mAh $g^{-1}$. The enhanced rate performance of skinned cathode indicated the promoted kinetics under elevated temperature. Such beneficial effect of ANC/graphene skin was further investigated in more detail by evaluating the Mn quantity on the LMO surface after 300 cycles at 60°C using TOF-SIMS. In Figure 5d, $Mn^+$ ions, which showed different trends from the surface to the bulk of LMO. Different from $^6Li^+$ profiles (Figure S17) that are consistent in all depths, here the intensity of $Mn^+$ was low at the LMO surface but increased drastically to a steady level in both pristine and

skinned cathodes. Compared to pristine cathode, ANC/graphene skinned cathode shows much larger amount of $Mn^{+}$ in the depth of 0-5 nm, indicating the better retained Mn content on the cathode surface, which is consistent to the previous Mn dissolution analysis in electrolyte.

## 4. Conclusions

A scalable and controllable skinning method, employing a commercial available sprayer, was formulated that improved thermal stability of the LMO-based cathodes in rechargeable hybrid aqueous lithium battery (ReHAB). Featuring the continuous coverage and the facile electron transport, ANC/graphene skinned cathode showed much better cycling stability (61% capacity retention after 300 cycles) at 60 °C in 1.15 mAh ReHABs, 200% larger than the retention of the battery without the hybrid skin. ANC/graphene skin on large cathodes (7 mAh cell) also showed similar performance improvement, indicating good scale-up potentials. Based on the impedance and XRD characterizations of fresh and cycled cathode, we proposed that ANC/graphene skin can significantly retard the undesired side reactions between the LMO and the aqueous electrolyte that retained charge transfer kinetics. ICP-AES and TOF-SIMS analysis results of Mn species in the electrolyte and the cathode surface further confirmed our hypothesis that the ANC/graphene skin greatly suppresses Mn dissolution into aqueous electrolyte. The facile polymer-skinning method proposed in this study makes LMO based aqueous battery possible in the application of EVs, opening a new avenue on cathode modifications in various aqueous energy storage systems.

**Author information**

**Corresponding Author**

*Email: p4chen@wuaterloo.ca

## References

[1] L. Lu, X. Han, J. Li, J. Hua, M. Ouyang, A review on the key issues for lithium-ion battery management in electric vehicles, Journal of power sources, 226 (2013) 272-288.
[2] A. Khaligh, Z. Li, Battery, ultracapacitor, fuel cell, and hybrid energy storage systems for electric, hybrid electric, fuel cell, and plug-in hybrid electric vehicles: State of the art, IEEE transactions on Vehicular Technology, 59 (2010) 2806-2814.
[3] W. Li, J.R. Dahn, D.S. Wainwright, Rechargeable Lithium Batteries with Aqueous Electrolytes, Science, 264 (1994) 1115-1118.
[4] H. Kim, J. Hong, K.-Y. Park, H. Kim, S.-W. Kim, K. Kang, Aqueous rechargeable Li and Na ion batteries, Chemical reviews, 114 (2014) 11788-11827.
[5] J.Y. Luo, Y.Y. Xia, Aqueous Lithium□ion Battery LiTi2 (PO4) 3/LiMn2O4 with High Power and Energy Densities as well as Superior Cycling Stability, Advanced Functional Materials, 17 (2007) 3877-3884.
[6] S. Zhang, Y. Li, C. Wu, F. Zheng, Y. Xie, Novel flowerlike metastable vanadium dioxide (B) micronanostructures: facile synthesis and application in aqueous lithium ion batteries, The Journal of Physical Chemistry C, 113 (2009) 15058-15067.
[7] P.-L. Taberna, S. Mitra, P. Poizot, P. Simon, J.-M. Tarascon, High rate capabilities Fe3O4-based Cu nano-architectured electrodes for lithium-ion battery applications, Nature materials, 5 (2006) 567-573.
[8] H.-W. Lee, P. Muralidharan, R. Ruffo, C.M. Mari, Y. Cui, D.K. Kim, Ultrathin spinel LiMn2O4 nanowires as high power cathode materials for Li-ion batteries, Nano letters, 10 (2010) 3852-3856.
[9] W. Tang, S. Tian, L. Liu, L. Li, H. Zhang, Y. Yue, Y. Bai, Y. Wu, K. Zhu, Nanochain LiMn 2 O 4 as ultra-fast cathode material for aqueous rechargeable lithium batteries, Electrochemistry Communications, 13 (2011) 205-208.
[10] H. Wang, K. Huang, Y. Zeng, S. Yang, L. Chen, Electrochemical properties of TiP 2 O 7 and LiTi 2 (PO 4) 3 as anode material for lithium ion battery with aqueous solution electrolyte, Electrochimica acta, 52 (2007) 3280-3285.
[11] D. Arumugam, G.P. Kalaignan, Synthesis and electrochemical characterizations of nano-SiO 2-coated LiMn 2 O 4 cathode materials for rechargeable lithium batteries, Journal of Electroanalytical Chemistry, 624 (2008) 197-204.
[12] J. Gnanaraj, V. Pol, A. Gedanken, D. Aurbach, Improving the high-temperature performance of LiMn 2 O 4 spinel electrodes by coating the active mass with MgO via a sonochemical method, Electrochemistry Communications, 5 (2003) 940-945.
[13] J. Tu, X. Zhao, J. Xie, G. Cao, D. Zhuang, T. Zhu, J. Tu, Enhanced low voltage cycling stability of LiMn 2 O 4 cathode by ZnO coating for lithium ion batteries, Journal of Alloys and Compounds, 432 (2007) 313-317.
[14] H. Liu, C. Cheng, Z. Hu, K. Zhang, Improving the elevated temperature performance of Li/LiMn 2 O 4 cells by coating with ZnO, Journal of materials science, 40 (2005) 5767-5769.
[15] J.-S. Kim, C. Johnson, J. Vaughey, S. Hackney, K. Walz, W. Zeltner, M. Anderson, M. Thackeray, The Electrochemical Stability of Spinel Electrodes Coated with ZrO2, Al2 O 3, and SiO2 from Colloidal Suspensions, Journal of The Electrochemical Society, 151 (2004) A1755-A1761.

[16] Z. Yang, W. Yang, D.G. Evans, Y. Zhao, X. Wei, The effect of a Co–Al mixed metal oxide coating on the elevated temperature performance of a LiMn 2 O 4 cathode material, Journal of Power Sources, 189 (2009) 1147-1153.
[17] J.-H. Cho, J.-H. Park, M.-H. Lee, H.-K. Song, S.-Y. Lee, A polymer electrolyte-skinned active material strategy toward high-voltage lithium ion batteries: a polyimide-coated LiNi 0.5 Mn 1.5 O 4 spinel cathode material case, Energy & Environmental Science, 5 (2012) 7124-7131.
[18] M. Yu, A. Wang, F. Tian, H. Song, Y. Wang, C. Li, J.-D. Hong, G. Shi, Dual-protection of a graphene-sulfur composite by a compact graphene skin and an atomic layer deposited oxide coating for a lithium-sulfur battery, Nanoscale, 7 (2015) 5292-5298.
[19] T.K. Hoang, M. Acton, H.T. Chen, Y. Huang, T.N.L. Doan, P. Chen, Sustainable gel electrolyte containing Pb 2+ as corrosion inhibitor and dendrite suppressor for the zinc anode in the rechargeable hybrid aqueous battery, Materials Today Energy, 4 (2017) 34-40.
[20] T.K. Hoang, T.N.L. Doan, J.H. Cho, J.Y.J. Su, C. Lee, C. Lu, P. Chen, Sustainable Gel Electrolyte Containing Pyrazole as Corrosion Inhibitor and Dendrite Suppressor for Aqueous Zn/LiMn2O4 Battery, ChemSusChem, (2017).
[21] J. Yan, J. Wang, H. Liu, Z. Bakenov, D. Gosselink, P. Chen, Rechargeable hybrid aqueous batteries, Journal of Power Sources, 216 (2012) 222-226.
[22] X. Miao, H. Ni, X. Sha, T. Wang, J. Fang, G. Yang, Preparation of 0.4 Li2MnO3· 0.6 LiNi1/3Co1/3Mn1/3O2 with tunable morphologies via polyacrylonitrile as a template and applications in lithium□ion batteries, Journal of Applied Polymer Science, 133 (2016).
[23] A. Nilchi, R. Saberi, S.R. Garmarodi, A. Bagheri, Evaluation of PAN-based manganese dioxide composite for the sorptive removal of cesium-137 from aqueous solutions, Applied Radiation and Isotopes, 70 (2012) 369-374.
[24] R. Janus, P. Natkański, A. Wach, M. Drozdek, Z. Piwowarska, P. Cool, P. Kuśtrowski, Thermal transformation of polyacrylonitrile deposited on SBA-15 type silica: Effect on adsorption capacity of methyl–ethyl ketone vapor, Journal of thermal analysis and calorimetry, 110 (2012) 119-125.
[25] J. Li, K. Li, M. Li, D. Gosselink, Y. Zhang, P. Chen, A sulfur–polyacrylonitrile/graphene composite cathode for lithium batteries with excellent cyclability, Journal of Power Sources, 252 (2014) 107-112.
[26] J. Zhi, W. Zhao, X. Liu, A. Chen, Z. Liu, F. Huang, Highly conductive ordered mesoporous carbon based electrodes decorated by 3D graphene and 1D silver nanowire for flexible supercapacitor, Advanced Functional Materials, 24 (2014) 2013-2019.
[27] Y. Shin, A. Manthiram, Influence of the lattice parameter difference between the two cubic phases formed in the 4 V region on the capacity fading of spinel manganese oxides, Chemistry of materials, 15 (2003) 2954-2961.
[28] K. Xu, A. von Cresce, U. Lee, Differentiating contributions to “ion transfer” barrier from interphasial resistance and Li+ desolvation at electrolyte/graphite interface, Langmuir, 26 (2010) 11538-11543.
[29] J. Zhang, J. Wang, J. Yang, Y. NuLi, Artificial interface deriving from sacrificial tris (trimethylsilyl) phosphate additive for lithium rich cathode materials, Electrochimica Acta, 117 (2014) 99-104.
[30] X. Xiao, P. Lu, D. Ahn, Ultrathin multifunctional oxide coatings for lithium ion batteries, Advanced Materials, 23 (2011) 3911-3915.

[31] M. Li, X. Wang, Y. Yang, Z. Chang, Y. Wu, R. Holze, A dense cellulose-based membrane as a renewable host for gel polymer electrolyte of lithium ion batteries, Journal of Membrane Science, 476 (2015) 112-118.
[32] Y. Yang, Z. Chang, M. Li, X. Wang, Y. Wu, A sodium ion conducting gel polymer electrolyte, Solid State Ionics, 269 (2015) 1-7.
[33] Y. Zhu, S. Xiao, Y. Shi, Y. Yang, Y. Hou, Y. Wu, A composite gel polymer electrolyte with high performance based on poly (vinylidene fluoride) and polyborate for lithium ion batteries, Advanced Energy Materials, 4 (2014).
[34] Q. Liu, Z.-F. Li, Y. Liu, H. Zhang, Y. Ren, C.-J. Sun, W. Lu, Y. Zhou, L. Stanciu, E.A. Stach, Graphene-modified nanostructured vanadium pentoxide hybrids with extraordinary electrochemical performance for Li-ion batteries, Nature communications, 6 (2015) 6127.
[35] D. Aurbach, B. Markovsky, A. Rodkin, M. Cojocaru, E. Levi, H.-J. Kim, An analysis of rechargeable lithium-ion batteries after prolonged cycling, Electrochimica Acta, 47 (2002) 1899-1911.
[36] X. Zhu, Y. Yu, Y. Tian, K.E.K. Sun, H. Zhao, P. Chen, Enhancing rate performance of LiMn2O4 cathode in rechargeable hybrid aqueous battery by hierarchical carbon nanotube/acetylene black conductive pathways, Ionics, 22 (2016) 71-76.
[37] G. Wang, H. Zhang, L. Fu, B. Wang, Y. Wu, Aqueous rechargeable lithium battery (ARLB) based on LiV 3 O 8 and LiMn 2 O 4 with good cycling performance, Electrochemistry Communications, 9 (2007) 1873-1876.
[38] D. Zhou, S. Liu, H. Wang, G. Yan, Na 2 V 6 O 16· 0.14 H 2 O nanowires as a novel anode material for aqueous rechargeable lithium battery with good cycling performance, Journal of Power Sources, 227 (2013) 111-117.
[39] M. Zhao, Q. Zheng, F. Wang, W. Dai, X. Song, Electrochemical performance of high specific capacity of lithium-ion cell LiV 3 O 8//LiMn 2 O 4 with LiNO 3 aqueous solution electrolyte, Electrochimica Acta, 56 (2011) 3781-3784.
[40] H. Wang, Y. Zeng, K. Huang, S. Liu, L. Chen, Improvement of cycle performance of lithium ion cell LiMn 2 O 4/Li x V 2 O 5 with aqueous solution electrolyte by polypyrrole coating on anode, Electrochimica Acta, 52 (2007) 5102-5107.
[41] J. Zhi, A.Z. Yazdi, G. Valappil, J. Haime, P. Chen, Artificial solid electrolyte interphase for aqueous lithium energy storage systems, Science advances, 3 (2017) e1701010.
[42] L.n. Madec, J. Xia, R.m. Petibon, K.J. Nelson, J.-P. Sun, I.G. Hill, J.R. Dahn, Effect of sulfate electrolyte additives on LiNi1/3Mn1/3Co1/3O2/graphite pouch cell lifetime: correlation between XPS surface studies and electrochemical test results, The Journal of Physical Chemistry C, 118 (2014) 29608-29622.
[43] P. Xue, D. Gao, S. Chen, S. Zhao, B. Wang, L. Li, Improved high-temperature capacity retention of the LiMn 2 O 4 cathode lithium-ion battery by ion exchange polymer coating, RSC Advances, 4 (2014) 52624-52628.
[44] V. Vishwakarma, C. Waghela, Z. Wei, R. Prasher, S.C. Nagpure, J. Li, F. Liu, C. Daniel, A. Jain, Heat transfer enhancement in a lithium-ion cell through improved material-level thermal transport, Journal of Power Sources, 300 (2015) 123-131.
[45] M. Cooper, B. Mikic, M. Yovanovich, Thermal contact conductance, International Journal of heat and mass transfer, 12 (1969) 279-300.
[46] F. Gao, Z. Tang, Kinetic behavior of LiFePO 4/C cathode material for lithium-ion batteries, Electrochimica Acta, 53 (2008) 5071-5075.

[47] K.N. Wood, M. Noked, N.P. Dasgupta, Lithium metal anodes: toward an improved understanding of coupled morphological, electrochemical, and mechanical behavior, ACS Energy Letters, 2 (2017) 664-672.
[48] J. Zhi, S. Deng, Y. Zhang, Y. Wang, A. Hu, Embedding Co 3 O 4 nanoparticles in SBA-15 supported carbon nanomembrane for advanced supercapacitor materials, Journal of Materials Chemistry A, 1 (2013) 3171-3176.
[49] J. Zhi, H. Cui, A. Chen, Y. Xie, F. Huang, Efficient highly flexible dye sensitized solar cells of three dimensional graphene decorated titanium dioxide nanoparticles on plastic substrate, Journal of Power Sources, 281 (2015) 404-410.
[50] C. Wessells, R. Ruffo, R.A. Huggins, Y. Cui, Investigations of the electrochemical stability of aqueous electrolytes for lithium battery applications, Electrochemical and Solid-State Letters, 13 (2010) A59-A61.
[51] L. Suo, O. Borodin, T. Gao, M. Olguin, J. Ho, X. Fan, C. Luo, C. Wang, K. Xu, "Water-in-salt" electrolyte enables high-voltage aqueous lithium-ion chemistries, Science, 350 (2015) 938-943.
[52] J. Dahn, E. Fuller, M. Obrovac, U. Von Sacken, Thermal stability of LixCoO2, LixNiO2 and λ-MnO2 and consequences for the safety of Li-ion cells, Solid State Ionics, 69 (1994) 265-270.
[53] J.E. Greedan, N. Raju, A. Wills, C. Morin, S. Shaw, J. Reimers, Structure and magnetism in λ-MnO2. Geometric frustration in a defect spinel, Chemistry of materials, 10 (1998) 3058-3067.

ACCEPTED MANUSCRIPT

**Table 1**. A comparison of the cycling stability of various rechargeable lithium battery systems under elevated temperature

| Cathode | Anode | Electrolyte | Cycles | Capacity retention (%) | Ref. |
|---|---|---|---|---|---|
| $LiMn_2O_4$/CNT | Zn | 2M $Li_2SO_4$+1M $ZnSO_4$ | 300 | 68 | 33 |
| $LiMn_2O_4$ | $LiV_3O_8$ | 2M $Li_2SO_4$ | 100 | 53 | 34 |
| $LiMn_2O_4$ | $Na_2V_6O_{16}\cdot 0.14 H_2O$ | Saturated $Li_2SO_4$ | 200 | 77 | 35 |
| $LiMn_2O_4$ | Zn | $Pb^{2+}$ containing gel | 300 | 75 | 19 |
| $LiMn_2O_4$ | $LiV_3O_8$ | Saturated $LiNO_3$ | 42 | 83 | 36 |
| $LiMn_2O_4$ | $Li_xV_2O_5$/PPy | 5 M $LiNO_3$ | 60 | 82 | 37 |
| $LiMn_2O_4$/RGO | Zn | 2M $Li_2SO_4$+1M $ZnSO_4$ | 100 | 73 | 38 |
| $LiNi_{1/3}Mn_{1/3}Co_{1/3}O_2$ | Graphite | 1 M $LiPF_6$ (EC/DMC) | 750 | 80 | 39 |
| $LiMn_2O_4$ | Li | 1 M $LiPF_6$ (EC/EMC) | 100 | 20 | 40 |
| PAN/graphene skinned $LiMn_2O_4$/Zn | M $Li_2SO_4$ + 2M $ZnSO_4$ (aqueous) | M $Li_2SO_4$ + 2M $ZnSO_4$ (aqueous) | 300 | 61 | This work |

ACCEPTED MANUSCRIPT

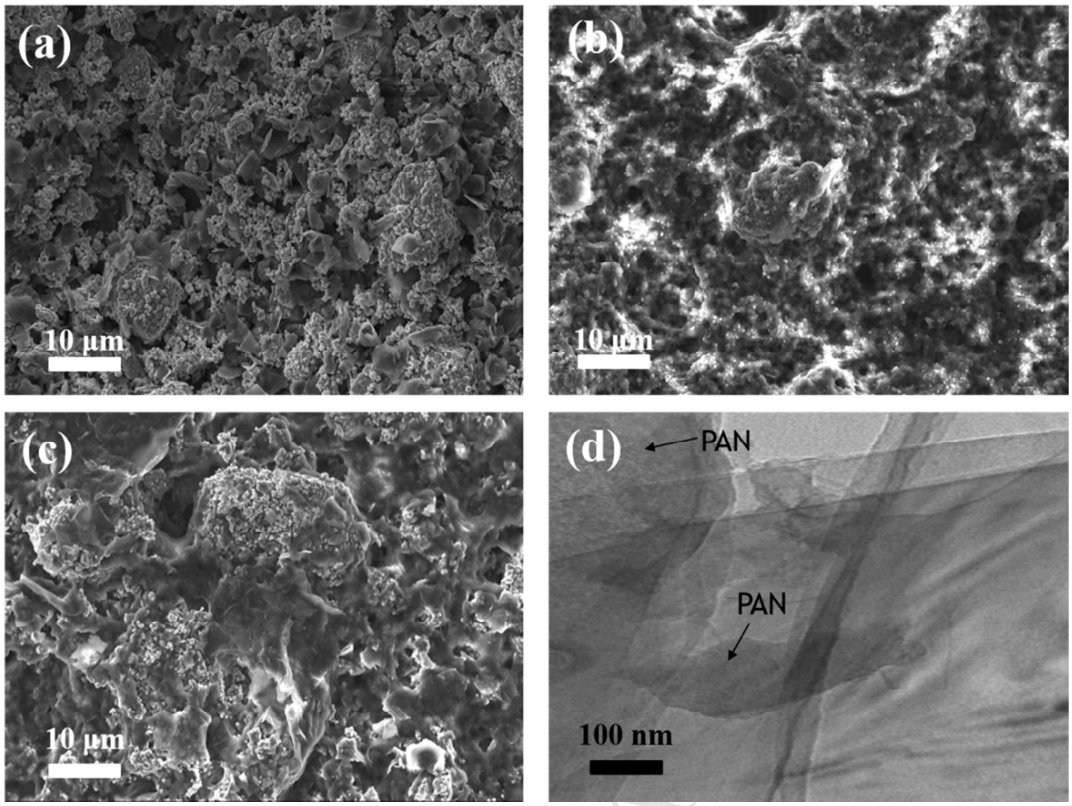


**Figure 1**. (a-c) SEM images of pristine, ANC skinned and ANC/graphene skinned cathodes, respectively. (d) TEM image of ANC/graphene skin.

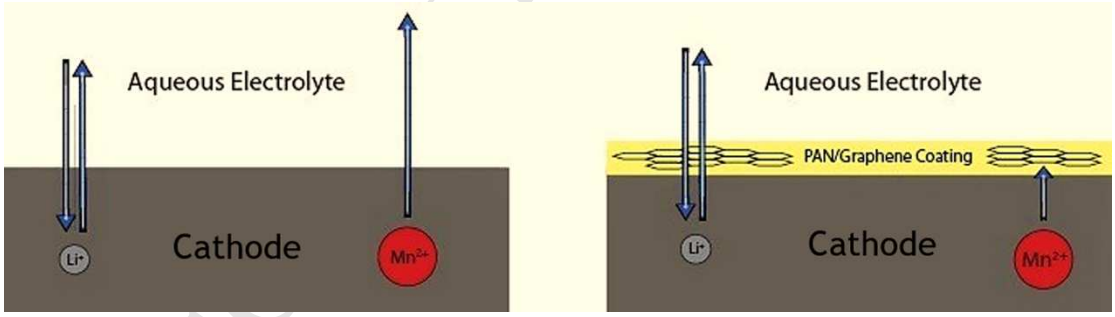


**Scheme 1**. Schematic illustration of ANC/graphene skin on the surface of LMO cathode and its role in suppressing the undesired interfacial reactions.

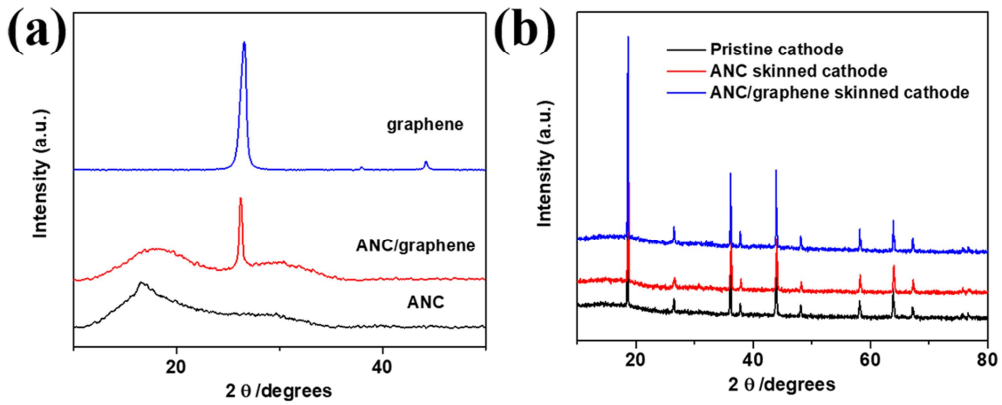


**Figure 2**. (a) XRD patterns of ANC, ANC/graphene skin and graphene. (b) XRD patterns of pristine LMO cathode, as well as ANC and ANC/graphene skinned LMO cathodes.

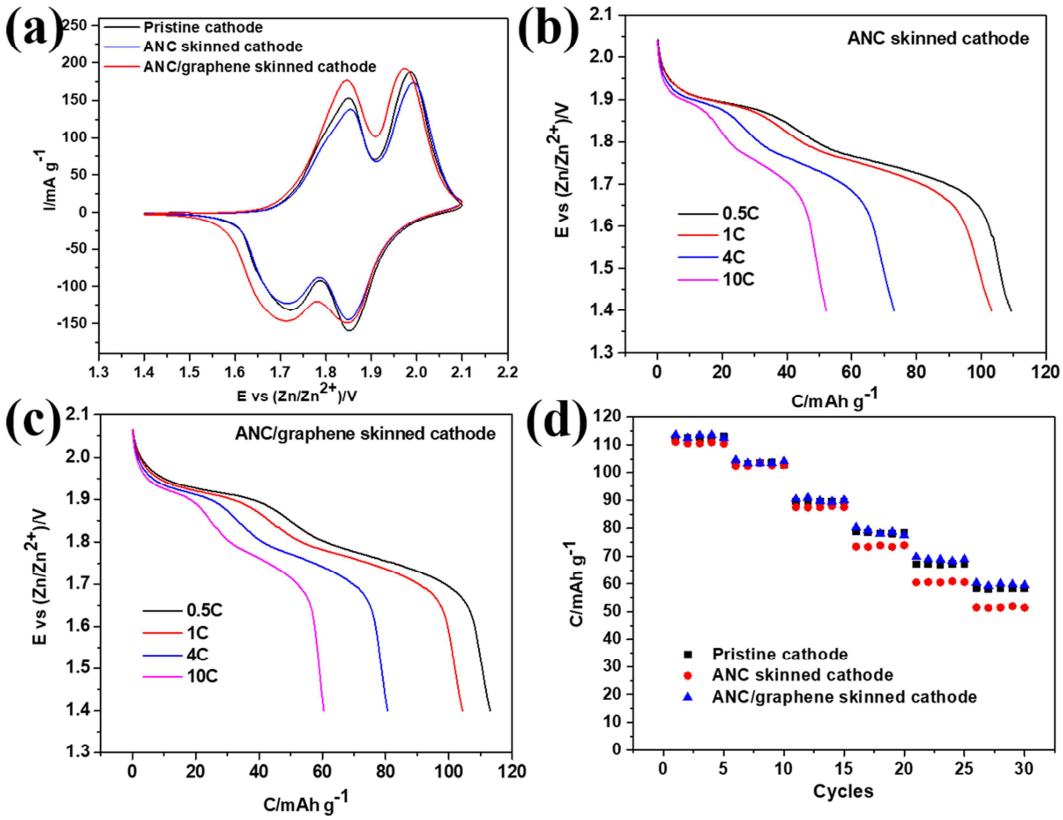


**Figure 3**. (a) Cyclic voltammetry (CV) results of ANC and ANC/graphene skinned cathodes, in comparison with pristine cathode. (b,c) Discharge profiles of ANC and

ANC/graphene skinned cathodes. (d) Comparison of discharge C-rate capabilities of ANC and ANC/graphene skinned cathodes with pristine one.

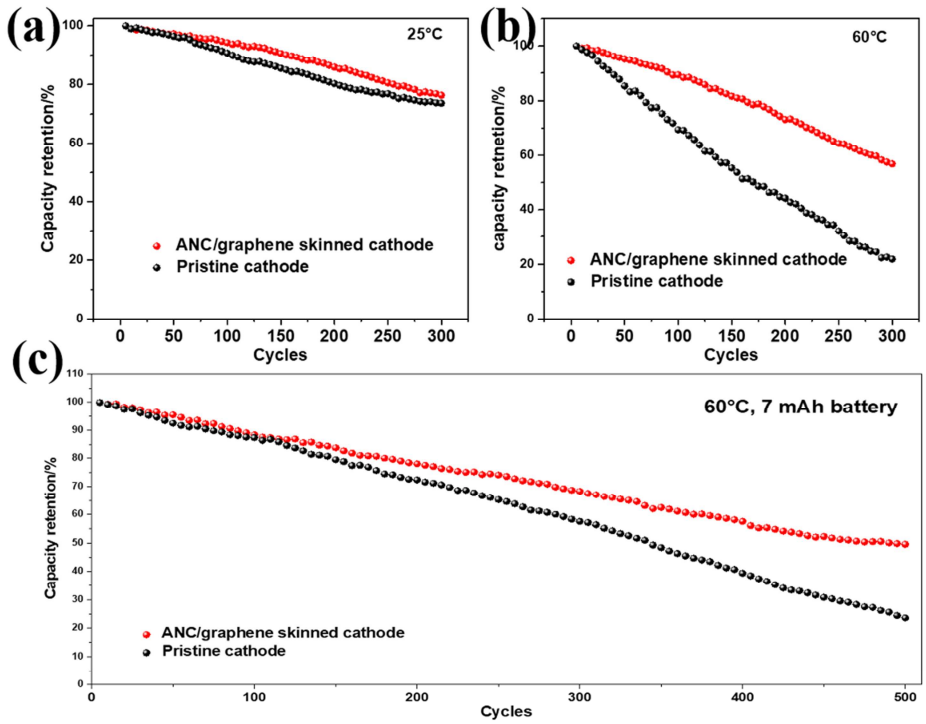


**Figure 4**. (a,b) Discharge capacities along with cycle number for ReHABs with pristine or ANC/graphene skinned cathodes: (a) at room temperature; (b) at 60°C. (c) Cyclability of 7 mAh ReHAB assembled with pristine or ANC/graphene skinned cathodes at 60°C.

ACCEPTED

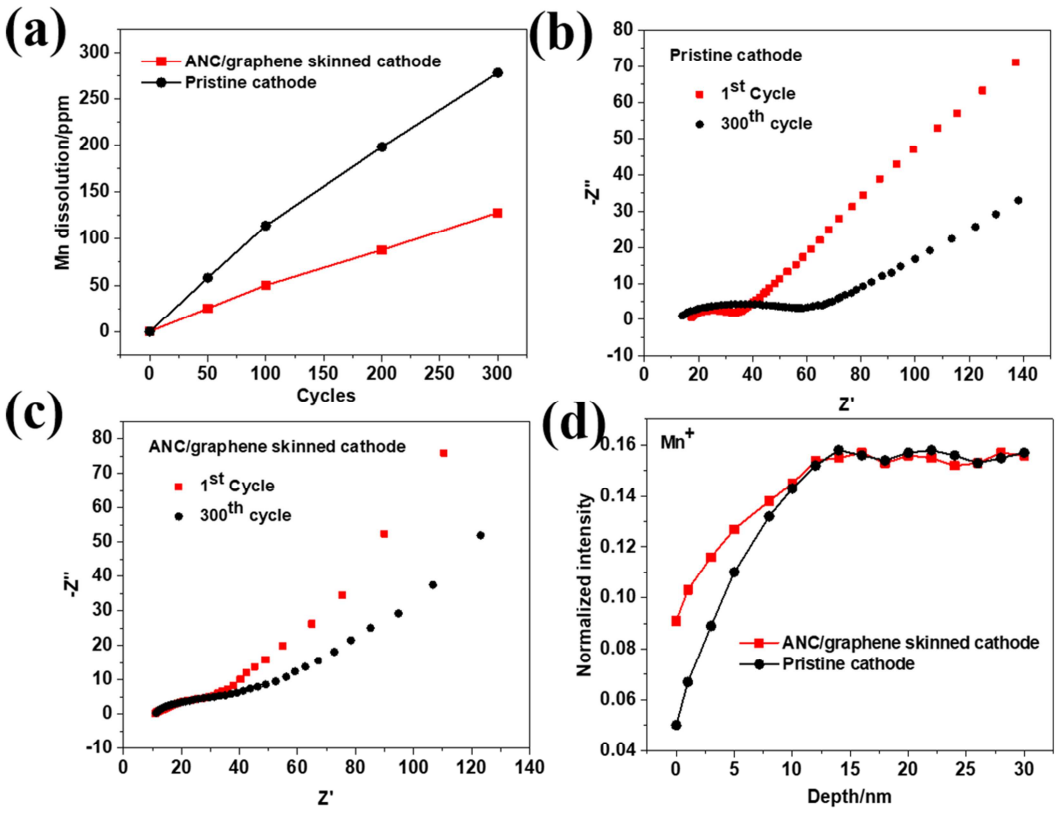


**Figure 5.** (a) Mn dissolution into aqueous electrolyte along with cycle numbers at 60 °C in ReHABs assembled with pristine and ANC/graphene skinned cathodes. (b,c) Changes in AC impedance spectra ($1^{st}$ and $300^{th}$ cycle) of ReHABs fabricated with: (b) pristine and (c) ANC/graphene skinned LMO cathodes. (d) Depth profiles of $Mn^{+}$ content obtained by TOF-SIMS (normalized by that of $Li^{+}$ in pristine and ANC/graphene skinned cathodes.

ACCEPTED MANUSCRIPT

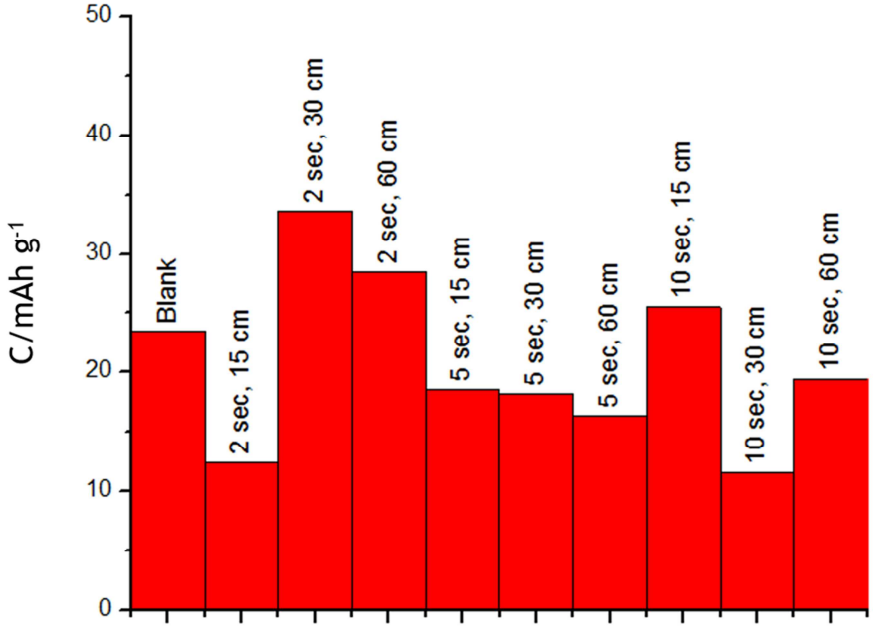


**Figure S1**. Capacity loss during float charge from various spraying methods

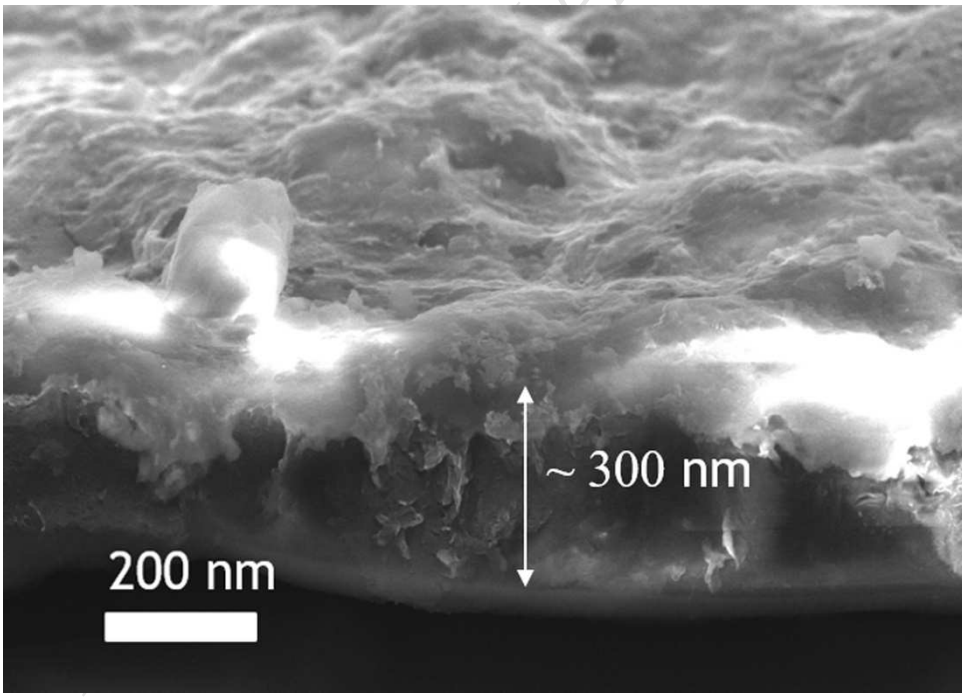


**Figure S2**. Cross-sectional SEM image of ANC/graphene skinned silica substrate.

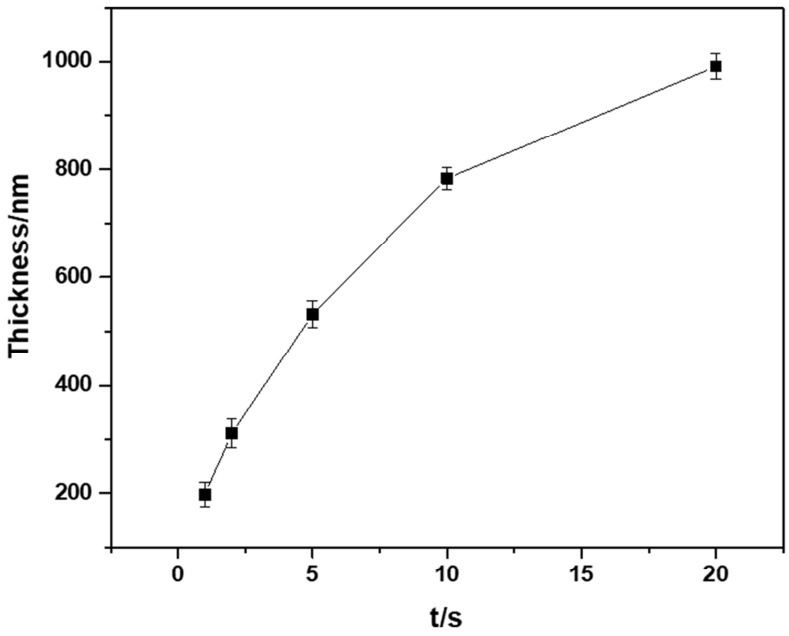


**Figure S3**. Thickness of ANC/graphene skin on silica substrate as a function of spraying time (the distance from nozzle to cathode was fixed to 15 cm).

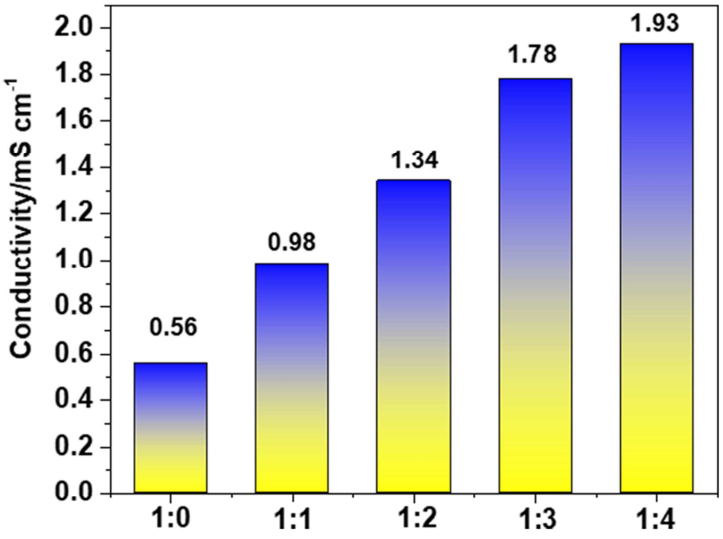


**Figure S4**. Electrical conductivities of ANC/graphene skin with different mass ratios (1:x, $mass_{ANC}$ : $mass_{graphene}$).

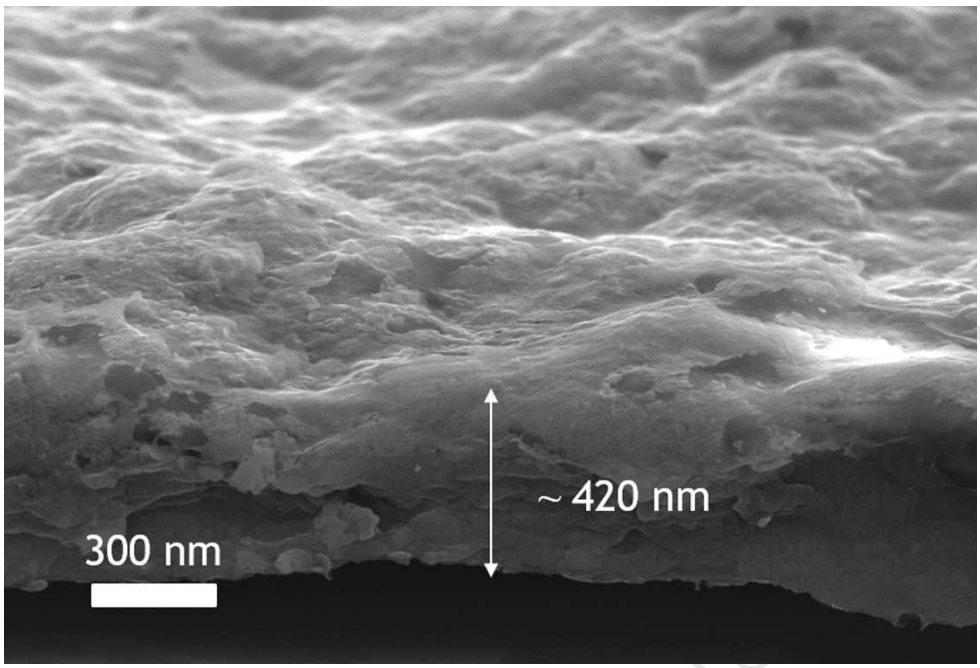


**Figure S5**. Cross-sectional SEM image of ANC/graphene skinned silica substrate immersed in aqueous electrolyte (2M $ZnSO_4$ and 1M $Li_2SO_4$) for 24 hours at 20°C.

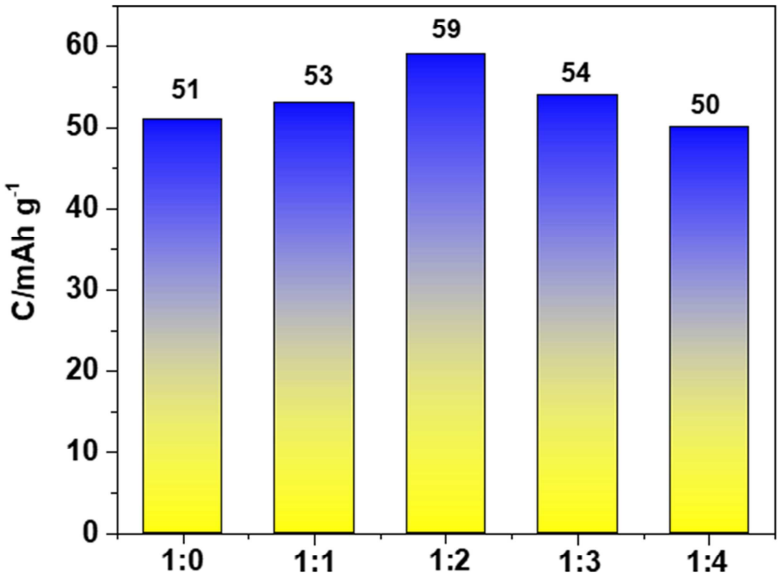


**Figure S6**. 10C discharge capacity of ANC/graphene skinned cathodes under different ANC/graphene mass ratios (1:x, $mass_{ANC}$ : $mass_{graphene}$).

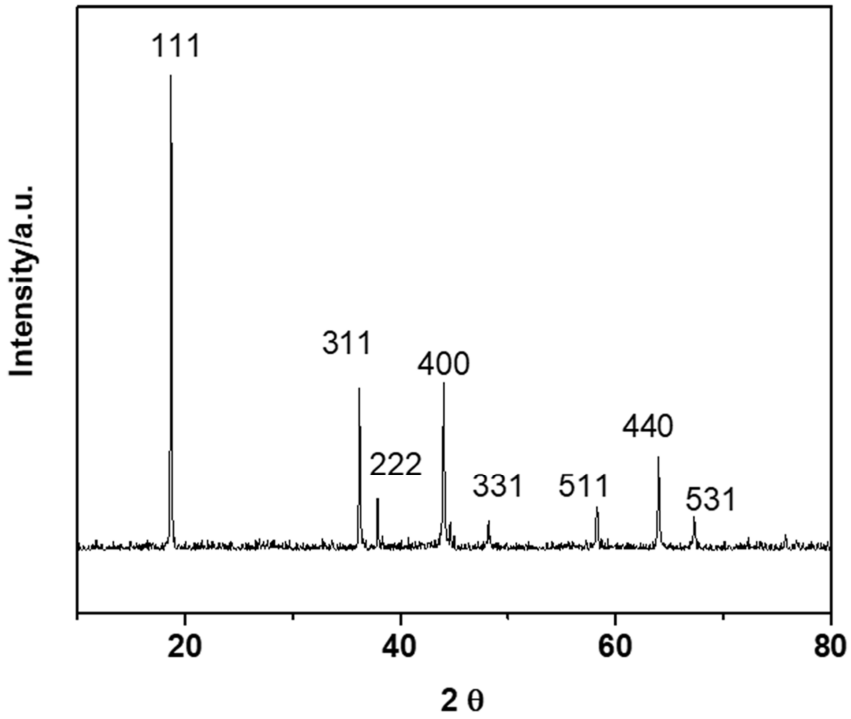


**Figure S7**. XRD patterns of powders scraped from ANC/graphene skinned cathode after 300 cycles at 60°C. All the peaks are well indexed with spinel $LiMn_2O_4$ (PDF card No:35-0782) crystals, and no λ-MnO2 phases are observed.

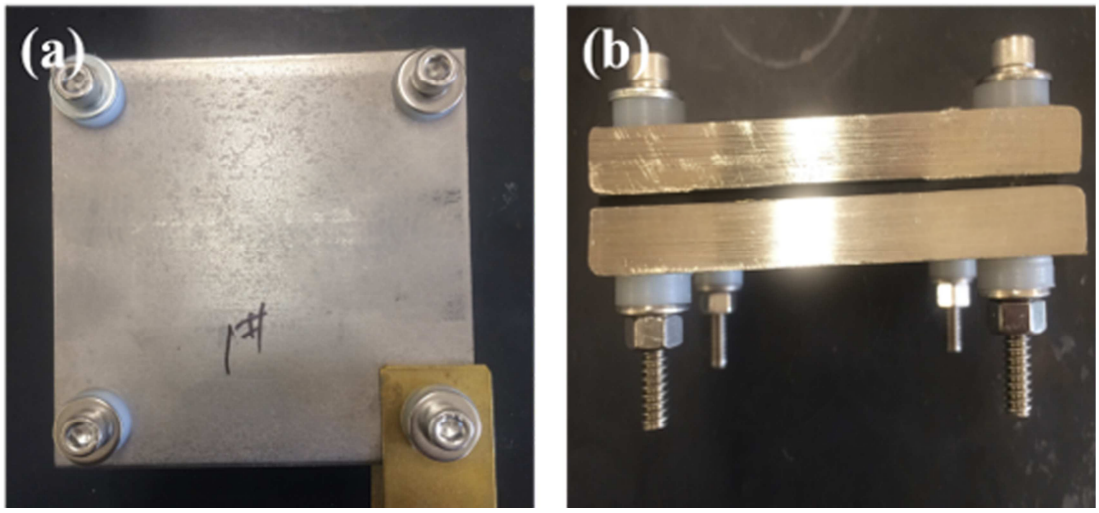


**Figure S8**. (a, b) Prototype of uninterruptible power system (7mAh) using 9 $cm^2$ large area cathode

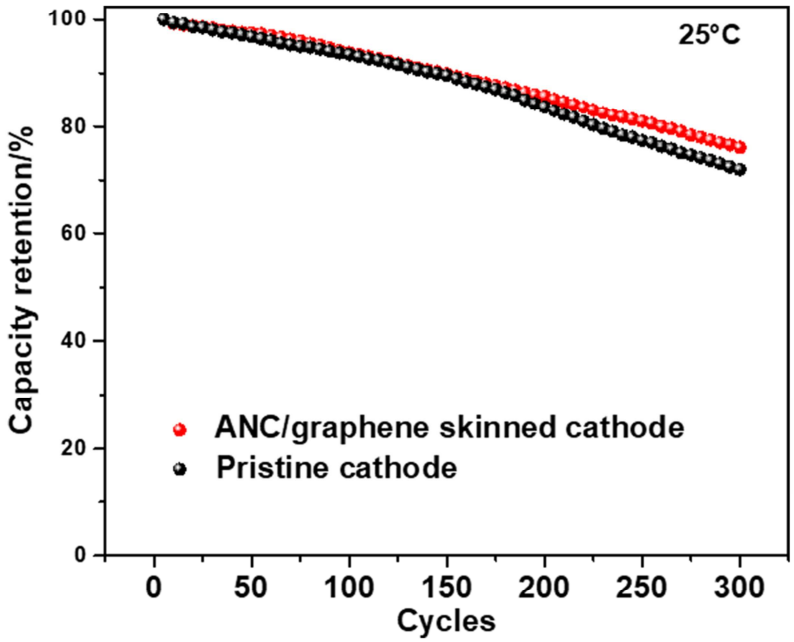


**Figure S9**. Cycling stability of skinned and pristine cathode in 7 mAh cell under room temperature.

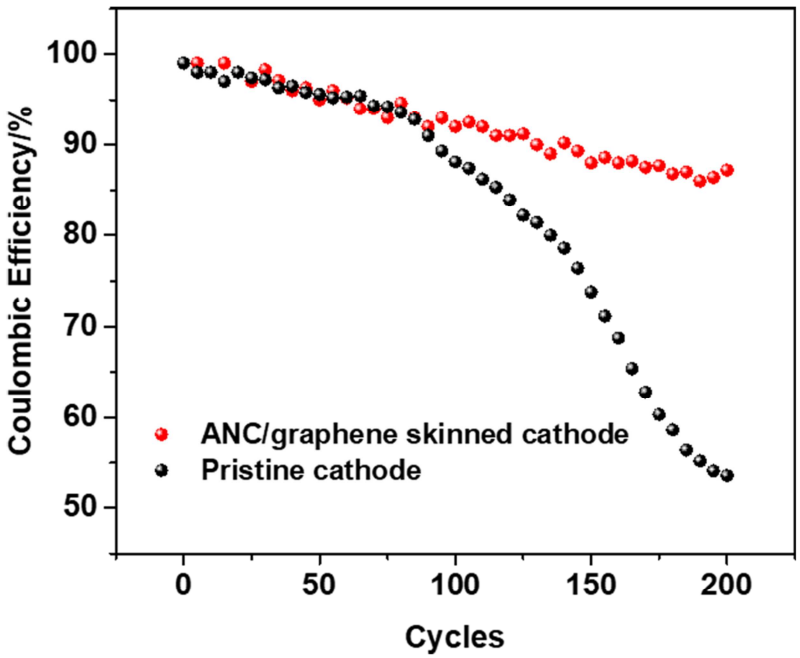


**Figure S10.** Coulombic efficiencies of ANC/graphene skinned and pristine cathodes in 7 mAh ReHAB at 60°C.

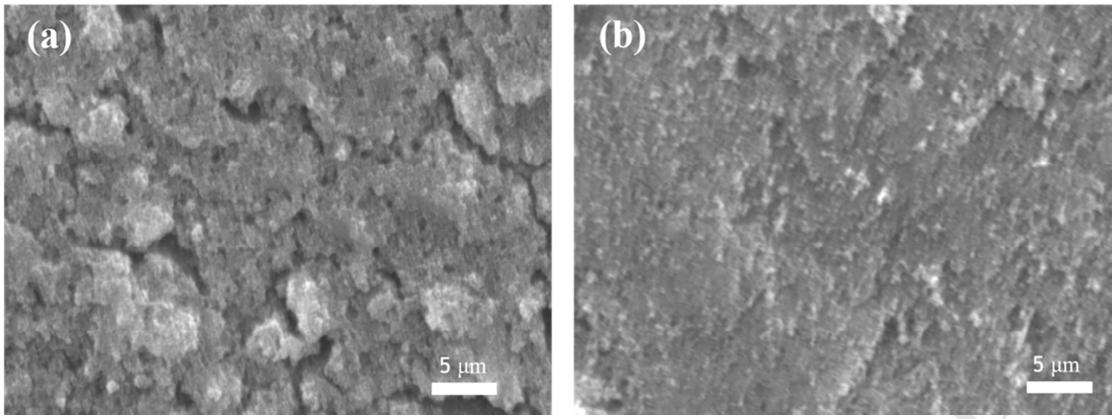


**Figure S11.** SEM images of Zn anodes with (a) pristine cathode and (b) ANC/graphene cathode from 7 mAh cells after 300 cycles under 60°C.

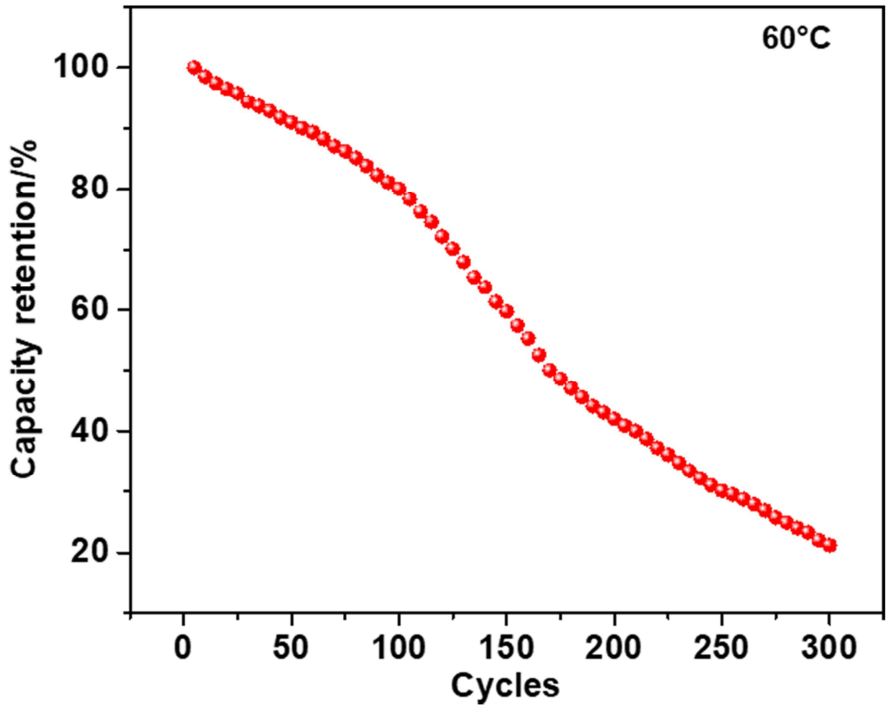


**Figure S12**. Cycling performance of 7 mAh cell with graphene coated cathode under 60°C

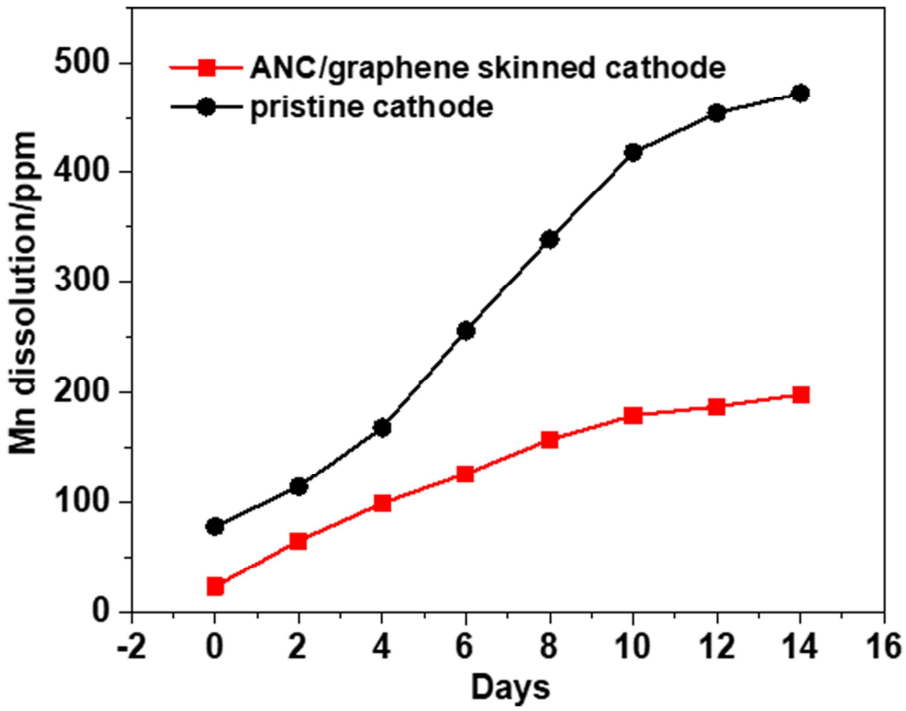


**Figure S13.** Mn dissolution into aqueous electrolyte along with cycle numbers at 60 °C in ReHABs assembled with pristine and ANC/graphene skinned cathodes.

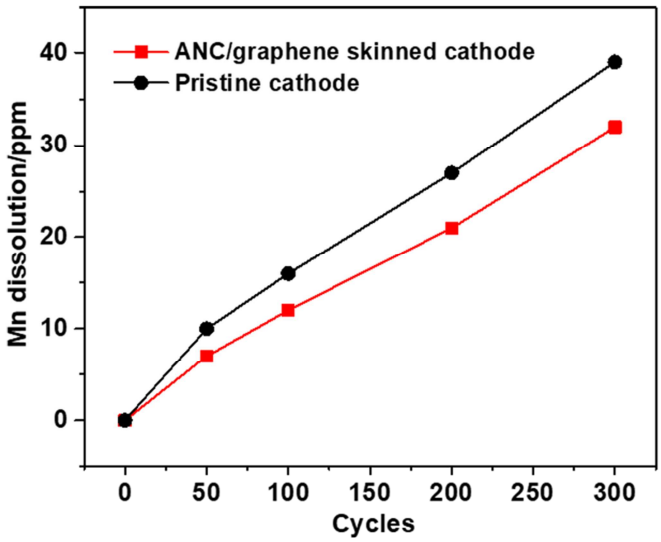


**Figure S14.** Mn dissolution into aqueous electrolyte along with cycle numbers at 25°C in ReHABs assembled with pristine and ANC/graphene skinned cathodes.

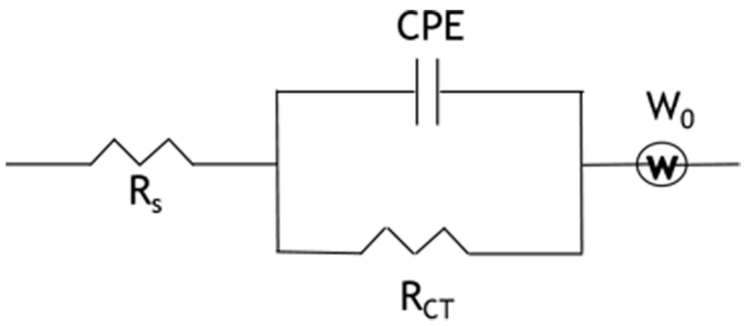


**Figure S15**. Corresponding equivalent circuit of EIS data as shown in Figure 5(b and c).

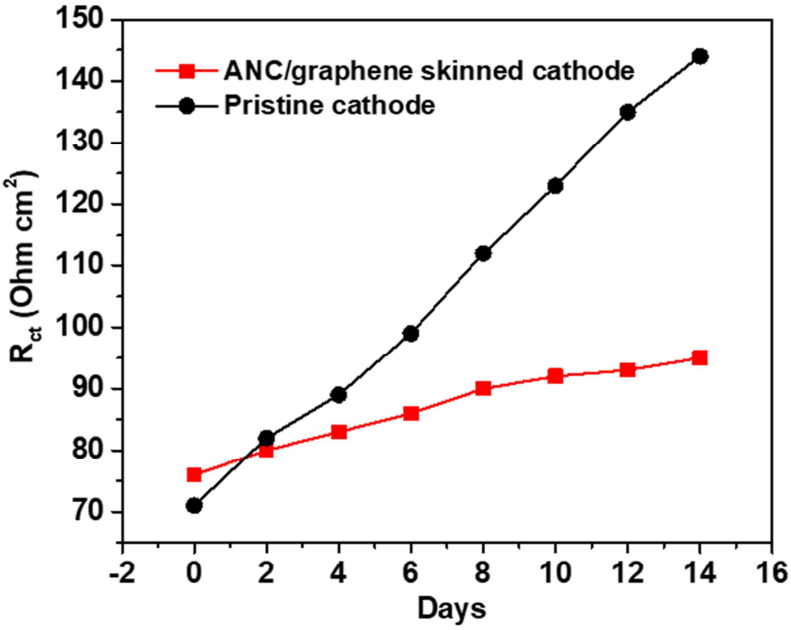


**Figure S16**. Evolution trends of $R_{ct}$ in pristine and ANC/graphene skinned cathodes along with storage time.

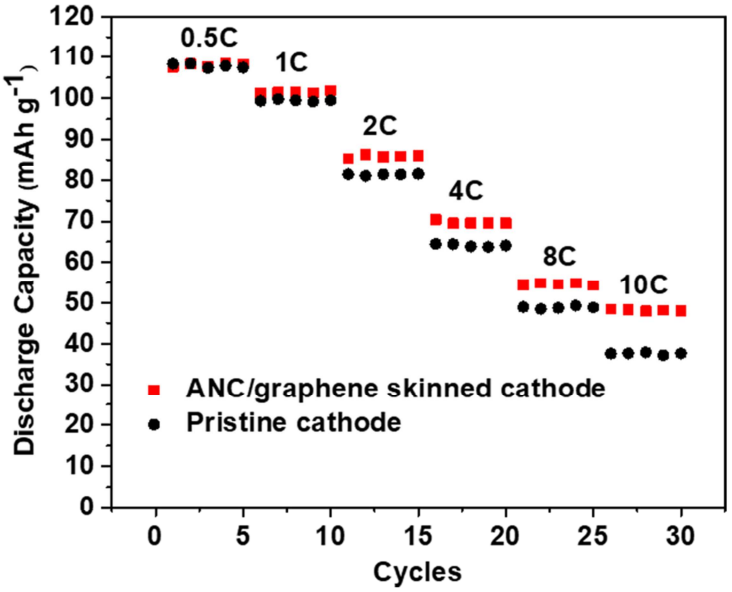


**Figure S17**. Rate capabilities of cells assembled with ANC/graphene skinned and pristine cathodes under 60 °C.

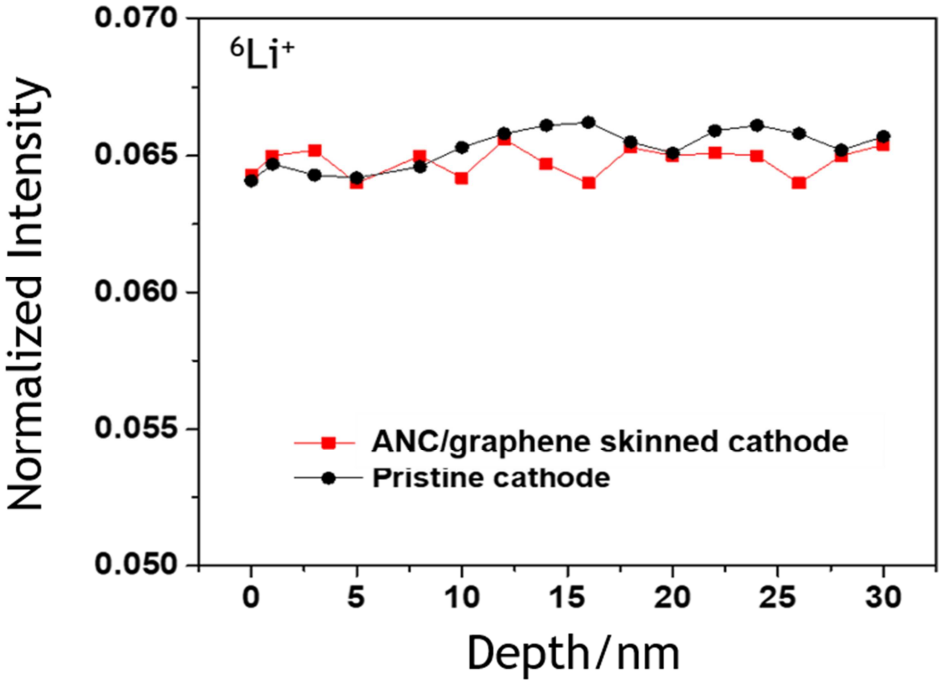


**Figure S18**. Depth profiles of $^{6}Li^{+}$ content obtained by TOF-SIMS in pristine and ANC/graphene skinned cathodes.